

# Experimental and numerical heat transfer studies on quenching of Inconel 600 probe

G. Ramesh · K. Narayan Prabhu

Received: 18 October 2013 / Accepted: 19 May 2014 / Published online: 12 June 2014  
© Springer-Verlag Berlin Heidelberg 2014

**Abstract** The effect of heat transfer coefficient and quench start temperature on cooling behaviour of Inconel 600 quench probe was assessed by numerical experiments. A quantitative model that relates the mean cooling rate and quench start temperature of the probe with the boundary heat transfer coefficient was proposed. Computed aided cooling curve analysis was carried out by heating Inconel 600 probe to temperatures varying from 100 to 850 °C followed by quenching in water. The results of quenching experiments and the data available in the literature were used to validate the proposed model. A good agreement between the measured and estimated value was observed. The results showed that the film and transition boiling of cooling stages were significantly influenced by quench start temperature of the material while nucleate boiling and convective cooling stages were strongly dependent on the boundary heat transfer coefficient.

## List of symbols

Bi	Biot number
$\rho$	Density (kg/m <sup>3</sup> )
q	Heat flux (W/m <sup>2</sup> )
CR	Mean cooling rate (°C/s)
h	Mean heat transfer coefficient (W/m <sup>2</sup> K)
$h_{\max}$	Peak heat transfer coefficient (W/m <sup>2</sup> K)
$T_{\text{start}}$	Probe quench start temperature (°C)
$T_{\text{q}}$	Quenchant temperature (°C)
r	Radial location (m)

$C_p$	Specific heat (J/kg K)
$T_s$	Surface temperature (°C)
k	Thermal conductivity (W/mK)
t	Time (s)

## 1 Introduction

Many metallurgical processes involve cooling operations where heat is extracted from the hot metal. The common practice of cooling metal involves either the immersion of hot metal into a liquid pool or a liquid coming in contact with the hot metal surface. For example, quench hardening of steel involves direct immersion of the preheated metal into the quenchant; on the other hand continuous casting of steel involves spraying of quenchant onto the hot surface of metal in secondary cooling followed by natural/forced air cooling. In the first case, control over heat transfer during cooling is not possible whereas the desired heat transfer condition during cooling can be achieved by varying flow rate, turbulence and impingement pressures of the quenchant in the latter case [1, 2]. The cooling of the hot metal by liquid however occurs by three stages namely vapour blanket; nucleate boiling and convective cooling [3].

The cooling/heat transfer conditions during these metallurgical processes have a significant effect on phase transformation and stress/strain evolution and thus the final quality of the product in terms of metallurgical and mechanical properties and distortion/cracking of components [4]. Mayer et al. [5] studied the effect of cooling rate  $\lambda$  (defined as  $\lambda = (t_{800\text{ °C}} - t_{500\text{ °C}})/100$  in s) on microstructure formation and mechanical properties of steel grade X38CrMoV5-1 during quench hardening.

G. Ramesh · K. Narayan Prabhu (✉)  
Department of Metallurgical and Materials Engineering,  
National Institute of Technology Karnataka, Srinivasnagar,  
Mangalore, India  
e-mail: prabhukn\_2002@yahoo.co.in

During quenching of hot work tool steel an increase in  $\lambda$  value results in a martensitic/mixed bainitic-martensitic structure. Further, higher fracture toughness and tensile strength were obtained with a high  $\lambda$  value. Lower fracture toughness and tensile strength were associated with a low value of  $\lambda$ . Tszeng et al. [6] simulated the heat treating process of a SAE 1035 carbon steel ring of 394 mm ID  $\times$  588 mm OD  $\times$  120 mm height. Boundary heat transfer coefficient values of 5 and 15 kW/m<sup>2</sup>K were used in simulation. Simulation results showed that a higher cooling rate was obtained with the assignment of high heat transfer coefficient which leads to higher levels of stress and more bainite and martensite in components. Sengupta et al. [7] discussed the role of cooling during continuous casting of metals. During secondary cooling of continuous casting, rapid cooling of solidifying metal resulting from excessive spraying of water can lead to large tensile strains at the surface of slab casting, which can open up small cracks formed in the primary cooling. The lower cooling by an insufficient spray of water can allow the slab to bulge out if the surface becomes too hot. This can lead to several defects, such as triple point cracks, midface cracks, midway cracks, centerline cracks and centre segregation. The heat transfer condition during metallurgical cooling processes should therefore be controlled to obtain improved properties of components.

During cooling, temperature of the hot metal starts decreasing from its initial value. Accordingly the cooling conditions of the component changes. The initial temperature of the component has a significant effect on the rate of heat transfer at the metal/quenchant interface. Further, the processing temperature is not the same for all metals. For example during quench/solution hardening, temperature at which the component cooled is 815–870 °C for steel, 400–590 °C for aluminium alloys, 775–1,000 °C for copper alloys, 385–566 °C for magnesium alloys, 980–1,175 °C for nickel alloys and 690–1,060 °C for titanium alloys [8]. Li et al. [9] investigated the influence of the initial sample start temperature on the boiling water heat transfer during water spray cooling of AISI 316 stainless steel having dimensions of 280 mm in diameter and 12.7 mm thick. The cooling experiments were conducted for the sample initial temperatures varying from 400 to 1,000 °C. The shape and magnitude of the boiling curve during transient cooling conditions was significantly influenced by the initial temperature of the material being cooled. Further, a noticeable drop in the peak heat flux with decreasing sample temperature was observed for samples with an initial temperature less than 500 °C. At temperatures at or above 700 °C, the peak heat flux was effectively independent of the initial temperature. Based on the test results, a simple method was proposed for predicting boiling curves under different start

temperatures. Babu and Kumar [10] carried out quenching experiments with 20 mm diameter and 50 mm length of a 304 L stainless steel probe heated to different initial soaking temperatures ranging from 400 to 950 °C in water to estimate the metal/quenchant heat flux transients. The heat flux transients showed a double peak. The first peak was observed immediately after the probe touched the water and the second peak occurred near the end of quenching when the surface of the probe reached nearly 100 °C. The first peak increased with a increase in the initial soaking temperature and occurred at different surface temperature and time. Maniruzzaman et al. [11] used Inconel 600 and SAE4140 steel quench probes to investigate the effect of quench start temperature on surface heat transfer coefficients. They conducted experiments with the quench start temperatures in the range of 850–450 °C at 100 °C interval for an Inconel probe and 900–400 °C at 50 °C interval for the SAE 4140 steel probe. Both probes heated to different temperatures were quenched in mineral oil. The results showed that the heat transfer coefficient not only depends on the part surface temperature, but also on the initial temperature of the quenched part. Further, the decrease in quench start temperature shifts the temperature for maximum heat transfer coefficient to lower temperatures. The literature suggests that the quench start temperature of the probe had significant influence on heat transfer conditions during quenching. Similarly, some of the other factors which affect heat transfer conditions at the metal/quenchant interface are (1) work-piece characteristics (composition, mass, geometry, surface roughness and condition) (2) quenchant characteristics (density, viscosity, specific heat, thermal conductivity, boiling temperature) and (3) quenching facility (bath temperature, agitation rate, flow direction) [2]. The previous research work by authors [12, 13] investigated the effect of boundary heat transfer coefficient on cooling curves during quenching. The average cooling rate increased almost linearly with boundary heat transfer coefficient at smaller diameter. The trend changes to exponential behaviour with increase in probe diameter for a low thermal conductivity probe. In the case of high thermal conductivity probe, the average cooling rate increased with heat transfer coefficient almost linearly for all probe diameters.

The development of a predictive model that correlates heat transfer condition and temperature of component therefore would be more useful for a process engineer to optimize cooling conditions and thus obtain desired properties. The present work was carried out with an objective to study and quantify the effect of varying boundary heat transfer coefficient and quench start temperature on cooling curves and cooling rate of the material during quenching process.

## 2 Materials and methods

### 2.1 Numerical experiments

For numerical simulation of cooling process, Inconel 600 was chosen as the quench probe material. The probe geometry was cylindrical with a diameter of 12.5 mm and length of 60 mm. Similarly, the boundary heat transfer coefficients ( $h$ ) varying from 500 to 10,000 W/m<sup>2</sup>K in step intervals of 500 W/m<sup>2</sup>K and probe initial quench start temperatures ( $T_{\text{start}}$ ) ranging from 100 to 850 °C in step intervals of 50 °C were selected for the simulation study. Simulations were carried out for all combinations of heat transfer coefficient and probe initial temperature using a finite difference heat transfer based SolidCast software package (Finite Solutions Inc., Slinger WI, USA). Virtual thermocouples were inserted at the geometric center (TC1) and at a location 2 mm from the surface to a depth of 30 mm (TC2). The time-temperature data was extracted from the thermal history file generated during simulation of cooling of the probe.

### 2.2 Quenching experiments

The quench probe of 12.5 mm diameter and 60 mm length was prepared from Inconel 600 material. Holes of 1 mm diameter were drilled to a depth of 30 mm at the probe geometric center (TC1) and at a location 2 mm from the surface of the quench probe (TC2). To obtain reproducible results, the quench probe was conditioned by heating and quenching in servoquench11 quench oil for several times. Calibrated K-type Inconel sheathed thermocouples were

inserted into the quench probe. Thermocouples were connected to a PC based temperature data acquisition system (NI PCI/PXI 4351). The probe was heated in a vertical tubular electric resistance furnace open at both ends and then transferred quickly to a vessel containing 2 litres of distilled water placed directly underneath the furnace. Quenching experiments were carried out at different probe initial temperatures ranging from 100 to 850 °C with an interval of 50 °C. The probe and quenchant temperatures were recorded for every 0.2 s interval during cooling. The schematic of the experimental setup is shown in Fig. 1.

### 2.3 Determination of the metal/quenchant heat flux transients

The metal/quenchant interfacial heat flux transients were estimated from the measured temperature histories and thermo-physical properties of probe material by solving the inverse heat conduction problem (IHCP). The equation that governs the two-dimensional transient heat conduction is given below.

$$\frac{1}{r} \frac{\partial}{\partial r} \left( kr \frac{\partial T}{\partial r} \right) + \frac{1}{r^2} \frac{\partial}{\partial \phi} \left( k \frac{\partial T}{\partial \phi} \right) = \rho C_p \frac{\partial T}{\partial t} \quad (1)$$

The above equation was solved inversely with appropriate initial and boundary conditions using the finite element based TmmFE inverse solver software (TherMet Solutions Pvt. Ltd., Bangalore, India), for estimating metal/quenchant heat transients. The mathematical description of the serial solution to IHCP is given in Ref. [14]. Figure 2 shows the solution domain of the quench probe used for estimation of the heat flux component. The geometry was

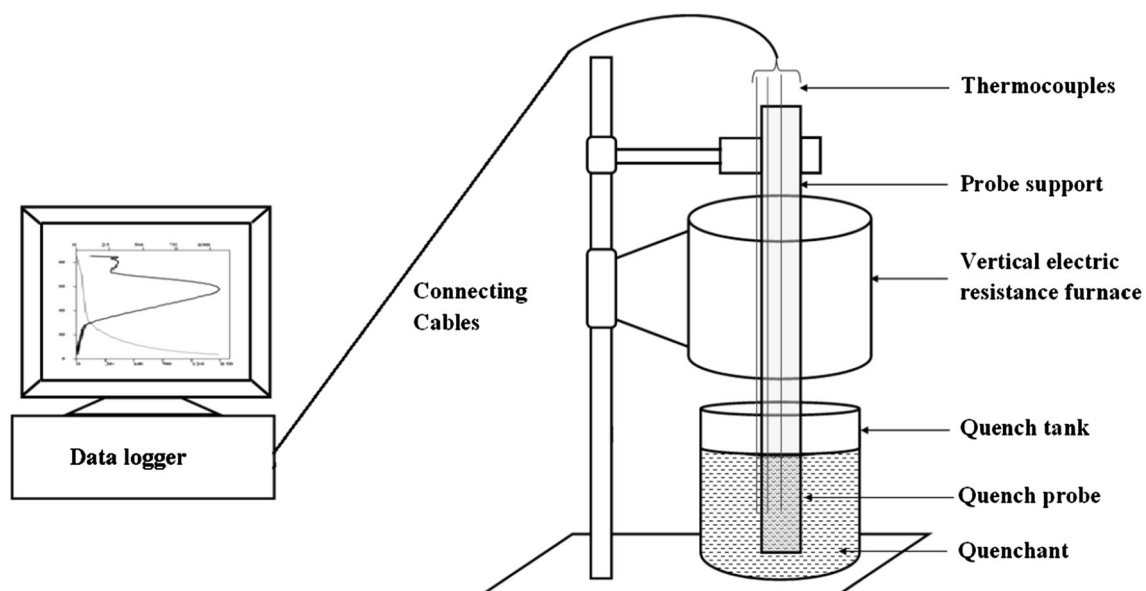


**Fig. 1** Schematic of experimental setup

discretized using a three node triangle and three side curved, uniform mesh. The total number of elements used in the present investigation was 625. The thermo-physical properties of probe material used in the inverse model are given in Table 1 [15]. An unknown heat flux boundary was assigned for metal/quenchant surface. The convergence limit for Gauss-Siedel iterations was set at  $10^{-6}$ .

### 3 Results and discussion

#### 3.1 Simulation of heat transfer during quenching

The temperature data estimated during quenching simulations was used to plot the cooling curve. Figure 3 shows a typical simulated cooling curve for a probe quench temperature of 800 °C and a boundary heat transfer coefficient of 2,500 W/m<sup>2</sup>K. Figure 4 shows the effect of probe quench start temperature and boundary heat transfer coefficient on the simulated cooling curves of the probe. The mean cooling rate (CR) was determined from the linear portion of the cooling curve. Figure 5 shows the mean cooling rate of the probe determined from the simulated cooling curve for two different quench temperatures at varying boundary heat transfer coefficients. It indicates that both initial quench temperature and boundary heat transfer coefficient had a significant effect on the cooling

rate of the probe. The mean cooling rate of the probe increases with quench start temperature and heat transfer coefficient. It was observed that the difference between the mean cooling rates at the TC1 and TC2 locations of the probe was minimum up to a certain intermediate heat transfer coefficient value and increased with the value of the heat transfer coefficient. Further, the critical value of *h* depends on the initial quench temperature of the probe. For example, difference between the mean cooling rates at the TC1 and TC2 locations of the probe was negligible below the heat transfer coefficient value of 1,500 W/m<sup>2</sup>K for the quench start temperature of 100 °C. The corresponding value for the quench start temperature of 850 °C was 3,500 W/m<sup>2</sup>K. The time-temperature data estimated for a particular heat transfer coefficients and probe quench start temperature was used to calculate temperature/time varying Biot number (defined as  $Bi = \frac{hR}{k}$ ). The mean Biot number ( $\overline{Bi}$ ) was then calculated using the following equation.

$$\overline{Bi} = \frac{1}{T_2 - T_1} \int_{T_1}^{T_2} Bi(T) dT \tag{2}$$

Figure 6 shows the effect of boundary heat transfer coefficient and quench start temperature of the probe on

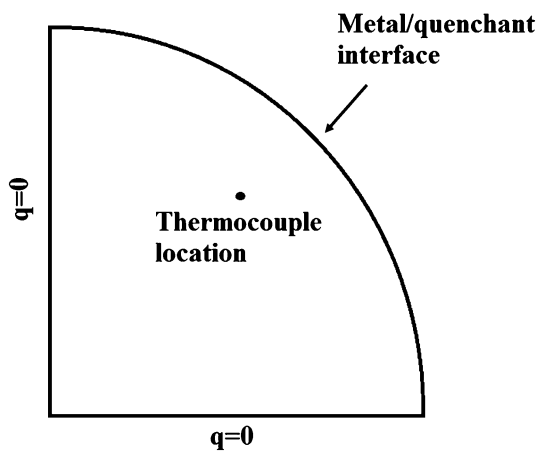


Fig. 2 Solution domain of quench probe used in IHCP

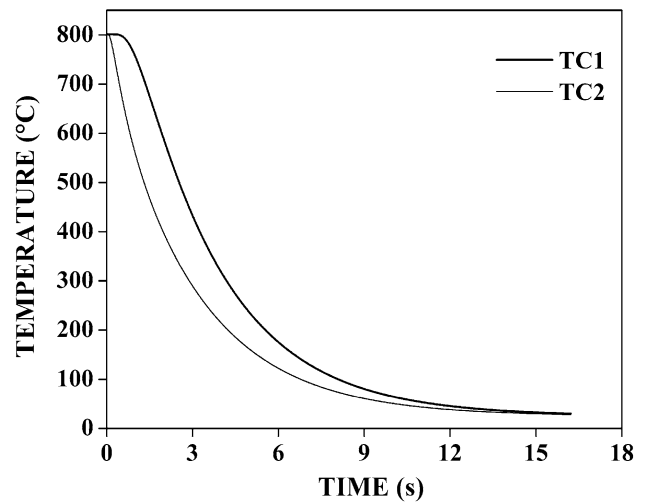
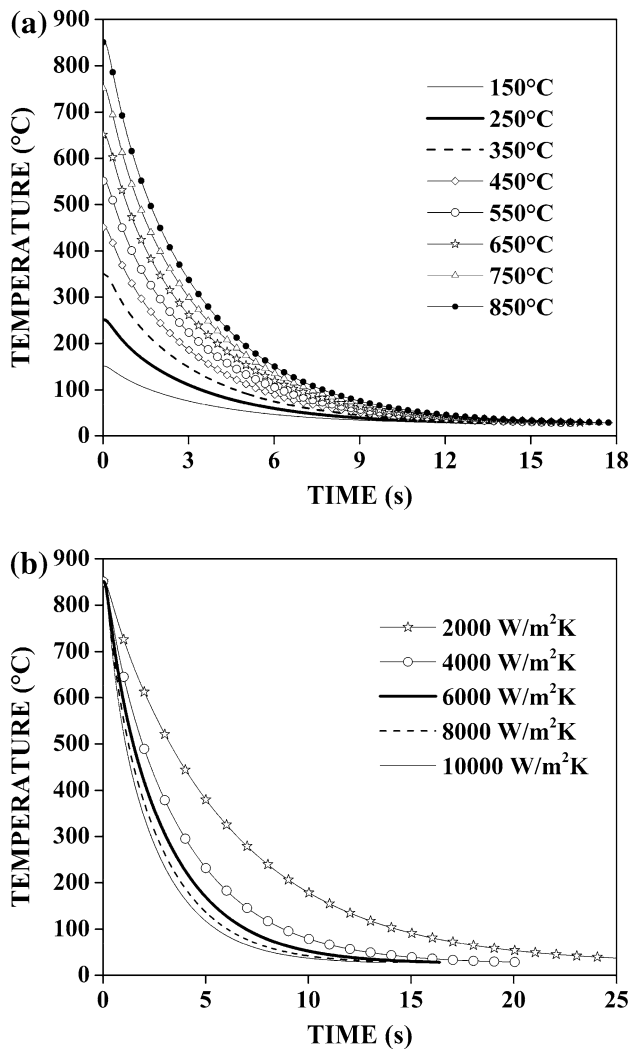


Fig. 3 Simulated cooling curves of probe cooled from 800 °C for the boundary heat transfer coefficient value of 2,500 W/m<sup>2</sup>K

Table 1 Thermo-physical properties of Inconel 600 used in IHCP [15]

Temperature (K)	323	373	423	473	523	573	623	673	723	773	873	973	1,073	1,173
Thermal conductivity (W/mK)	13.4	14.2	15.1	16	16.9	17.8	18.7	19.7	20.7	21.7	–	25.9	–	30.1
Specific heat (J/kgK)	451	467	–	491	–	509	–	522	–	533	591	597	597	611
Density (Kg/m <sup>3</sup> )	8,400	8,370	–	8,340	–	8,300	–	8,270	–	8,230	8,190	8,150	8,100	8,060



**Fig. 4** Effect of **a** quench start temperature of probe and **b** boundary heat transfer coefficient on simulated thermal histories of quench probe

mean Biot number. The mean Biot number increases with increase in heat transfer coefficients and decrease in the quench start temperature of the probe. The relationship between mean Biot number, heat transfer coefficient and quench start temperature was described according to the following equation.

$$\overline{Bi} = 0.234 + 1.933 \times 10^{-4} h - 5.275 \times 10^{-4} T_{start} \quad (3)$$

The coefficient of correlation for the above equation is 0.986. The temperature dependent critical values of  $h$  were input to Eq. (3) to estimate  $\overline{Bi}$  and found to vary in the band of 0.46–0.60 for quench start temperatures of the probe in the range of 100–850 °C. The critical Biot number was found to be 0.54. The isotherm during cooling of the probe showed one dimensional heat transfer throughout the section and variation of cooling rates within the probe was

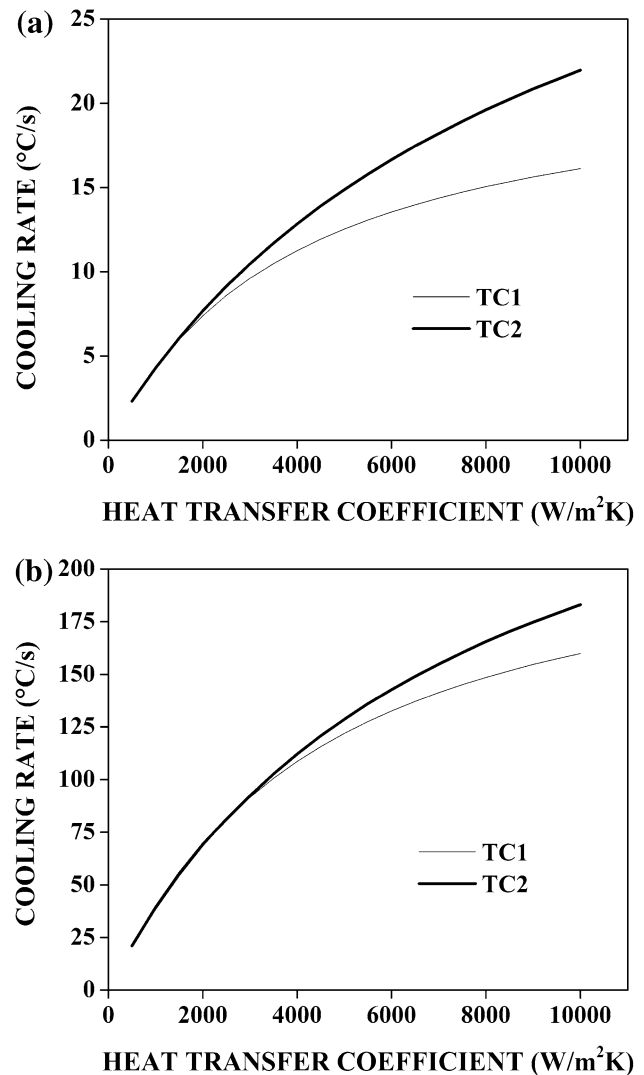


**Fig. 5** Effect of boundary heat transfer coefficients on mean cooling rate of probe for the probe quench start temperatures of **a** 100 °C and **b** 850 °C

minimum, below the critical Biot number 0.54. Above this value, the temperature gradient in the probe was significant. The temperature gradient and hence the evolution of thermal stresses during cooling of a component could be minimized by selection of the cooling condition at the surface of the component for which the Biot number is below the critical value.

The CR estimated for particular quench start temperature was normalized with respect to the value obtained for the  $h$  of 10,000 W/m²K ( $CR_{h10000}$ ). Figure 7 shows normalized cooling rate inside the probe at the TC2 location as a function of  $h$  for different quench start temperatures. The normalized cooling rate was found to vary with  $h$  for all quench start temperatures according to the following equation.

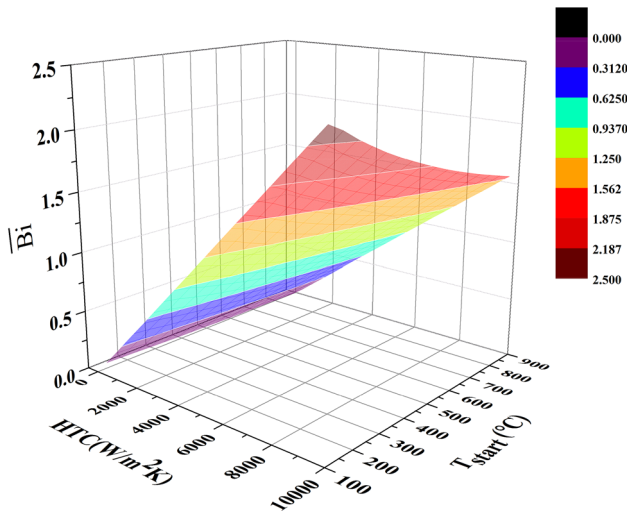


**Fig. 6** Effect of boundary heat transfer coefficient and quench start temperature of probe on mean Biot number

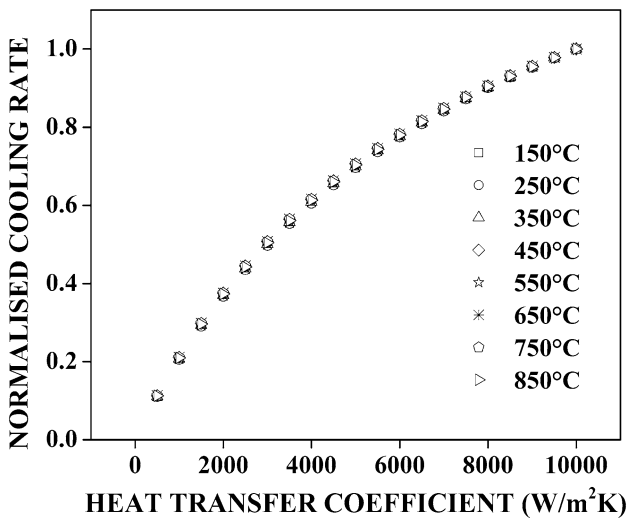


**Fig. 7** Normalized cooling rate of probe as a function of boundary heat transfer coefficient for different probe quench start temperatures

$$\frac{CR}{CR_{h10000}} = 0.06 + 1.65 \times 10^{-4}h - 7.23 \times 10^{-9}h^2 \quad (4)$$

The coefficient of correlation for the above equation was found to be 0.997. Similarly, the cooling rates estimated for a particular  $h$  were normalized with respect to the value obtained for the quench temperature of 850 °C ( $CR_{850\text{ }^\circ\text{C}}$ ). Figure 8 shows the normalized cooling rate inside the probe at the TC2 location as a function of quench start temperature for varying boundary  $h$  values. It was observed that the normalized cooling rate varies linearly with probe initial temperature ( $T_{start}$ ) for all values of  $h$  according to the following equation.

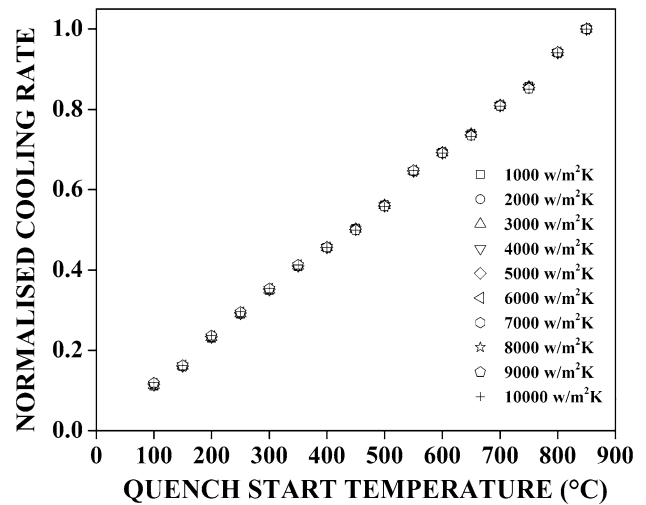


**Fig. 8** Normalized cooling rate of probe as a function of probe quench start temperature for varying boundary heat transfer coefficient

$$\frac{CR}{CR_{850\text{ }^\circ\text{C}}} = 0.00116T_{start} - 0.00537 \quad (5)$$

The coefficient of correlation for the above equation was found to be 0.998. The cooling rates estimated at the centre of the probe also showed a similar relationship with boundary  $h$  and quench start temperature. The cooling rate of all simulation experiments are presented in Fig. 9 which correlates boundary heat transfer coefficients, initial quench temperatures and mean cooling rates of the probe. The data was fitted according to the following equation

$$CR = A + Bh + CT_{start} + Dh^2 + ET_{start}^2 + FhT_{start} \quad (6)$$

where  $A$ ,  $B$ ,  $C$ ,  $D$ ,  $E$  and  $F$  are constants. The values of constants are given in Table 2. The coefficient of correlation for Eq. (6) is 0.99 indicating a good fit of data. The model is valid for  $h$  values from 500 to 10,000  $W/m^2K$  and  $T_{start}$  values from 100 to 850 °C.

### 3.2 Quenching experiments and validation

For validation of the above model, quenching experiments were carried out with an Inconel probe of same dimensions considered for the simulation study. The probe was heated to different temperatures ranging from 100 to 850 °C and quenched in distilled water. Experiments were repeated three times and the quench probe was monitored by quenching the probe at 850 °C in reference mineral oil (ServoQuench 11) after each set of experiments. Figure 10 shows thermal histories of the probe quenched in reference oil after each set of experiments indicating that the probe was not affected significantly after carrying out quenching. Figure 11 shows thermal histories of the probe heated to

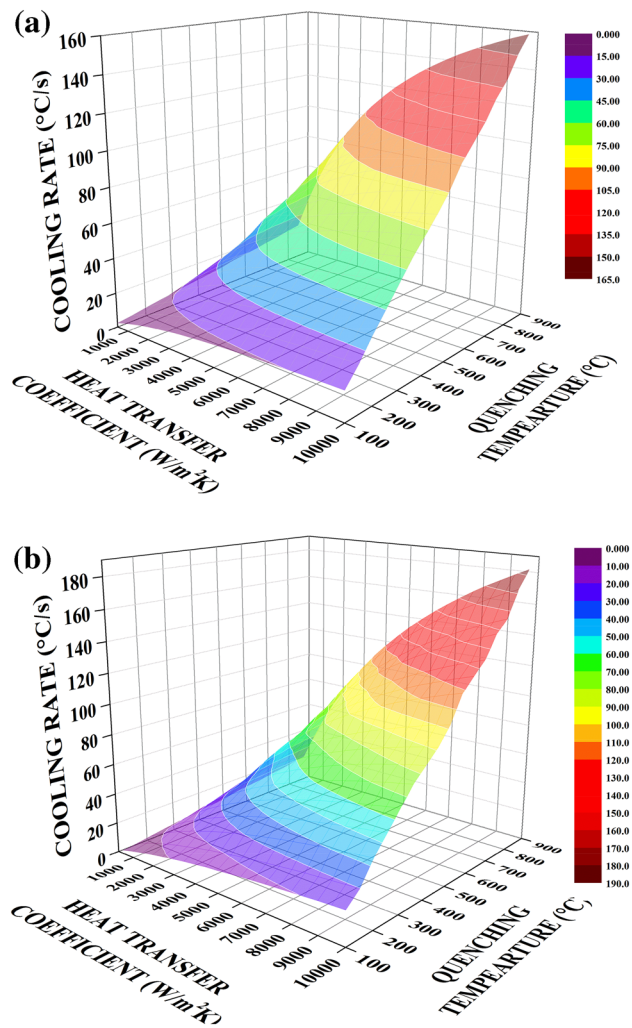


**Fig. 9** Effect of boundary heat transfer coefficient, quench start temperature on mean cooling rate at **a** TC1 and **b** TC2 locations of probe

**Table 2** Values of constants

Constant	For TC1 location	For TC2 location
A	-15.28524	-12.68865
B	0.00834	0.00772
C	0.04502	0.03226
D	$-8.21217 \times 10^{-7}$	$-7.34397 \times 10^{-7}$
E	$5.30209 \times 10^{-5}$	$1.1779 \times 10^{-5}$
F	$1.59968 \times 10^{-5}$	$1.86895 \times 10^{-5}$

different temperatures followed by quenching in water. The corresponding cooling rates are superimposed in Fig. 11. Grum et al. [16] reported a maximum cooling rate of around 200 °C/s and the temperature at which the peak occurred was in the interval between 650 and 500 °C at the center of an Inconel 600 probe heated to 850 °C during

water quenching. In the present study, the corresponding values were found to be 203 °C/s and 604 °C respectively. This indicates that experimental results are comparable with the data available in the literature. The thermal histories at the TC1 and TC2 locations of the probe follow the same behavior for all probe temperatures. The cooling curve shows a clear film boiling region for the probe quench temperatures of 850, 800 and 750 °C whereas no clear film boiling region was observed with the probe heated to the temperatures below 750 °C. The same behavior was also reported in references [9–11]. The transfer of heat from the interior to the surface of the probe was more than the amount of heat needed to evaporate the quenchant for the probe heated to a high temperature resulting in the formation of stable vapour film surrounding the surface of the quench probe. On the other hand, for lower quench start temperatures, the heat energy available at the surface of the probe was less than the energy required to evaporate the quenchant resulting in the absence of stable film formation during quenching. Quenching of the probe heated to different temperatures showed a peak cooling rate followed by a drop with a decrease in the probe temperature. The peak cooling rate and the temperature at which the peak cooling rate occur increased with an increase in the quench start temperature. For example, quenching of the probe heated to 600 °C showed peak cooling rate and temperature at peak cooling rate of 220 °C/s and 510 °C respectively measured at the TC2 location of probe. The corresponding values for quenching of the probe heated to 850 °C were 320 °C/s and 625 °C respectively. It was observed that the change in cooling rates with probe temperature were nearly the same after the occurrence of peak cooling rate for all quench start temperatures. Maniruzzaman et al. [11] carried out cooling curve analysis of an Inconel probe (12.5 mm dia  $\times$  60 mm length) heated to different temperatures followed by quenching in mineral oil. The cooling rate vs temperature plots (Fig. 12) showed a similar type of behavior to that observed in the present study. The magnitude of cooling rate was however very low. This was due to the use of mineral oil having low cooling severity compared to water used in the present study. The quench start temperature of the probe had influence only on the film and transition boiling of quenchant. On the other hand, cooling rate during nucleate boiling and convective cooling of quenchant was strongly dependent on the instantaneous probe temperature and was independent of the quench start temperature of the probe. The experimentally measured time-temperature data and thermo-physical properties of the quench probe were input to the inverse model to estimate the heat flux transients and surface temperature. The estimated heat flux transients for different quench start temperatures are shown in Fig. 13. The heat flux curve

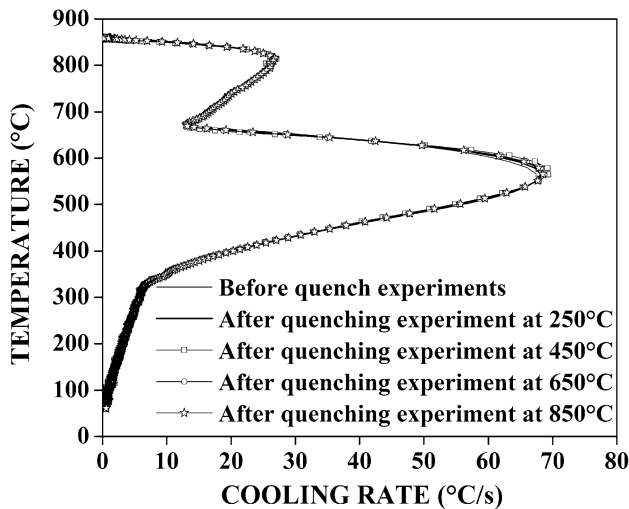


**Fig. 10** Cooling rate curves of quench probe against reference oil

shows a maximum shortly and then drops rapidly during cooling. The peak heat flux increases with an increase in the start temperature of quench probe. Quenching of the probe at high temperatures leads to more evaporation of quenchant and formation of vigorous bubble boiling at the probe surface resulting in higher heat flux at the metal/quenchant interface. However for a low quenching start temperature, the cooling of the probe is mainly by liquid cooling which resulted in the lower heat flux. The metal/quenchant heat transfer coefficient during quenching in water for different probe quench temperatures was determined by using the following equation.

$$h(t) = \frac{q(t)}{T_s(t) - T_q(t)} \quad (7)$$

Typical plots of the variation of heat transfer coefficient as a function of probe surface temperature during quenching of the probe heated to 800 and 400 °C in water are shown in Fig. 14. The peak  $h$  value of 12 kW/m<sup>2</sup>K was obtained for the probe heated to 850 °C quenched in water. Funatani et al. [17] reported a heat transfer coefficient of about 10 kW/m<sup>2</sup>K for an Inconel 600 probe heated to 850 °C quenched in water. The experimental results were comparable with the data reported in literature. The mean heat transfer coefficient values for the probe heated to different temperatures quenched in water were determined by using the following equation

$$h = \frac{1}{t_2 - t_1} \int_{t_1}^{t_2} h(t) dt \quad (8)$$

where  $t_1$  and  $t_2$  are the corresponding times used to determine the mean cooling rates. The determined  $h$  values and corresponding quench start temperatures of the probe

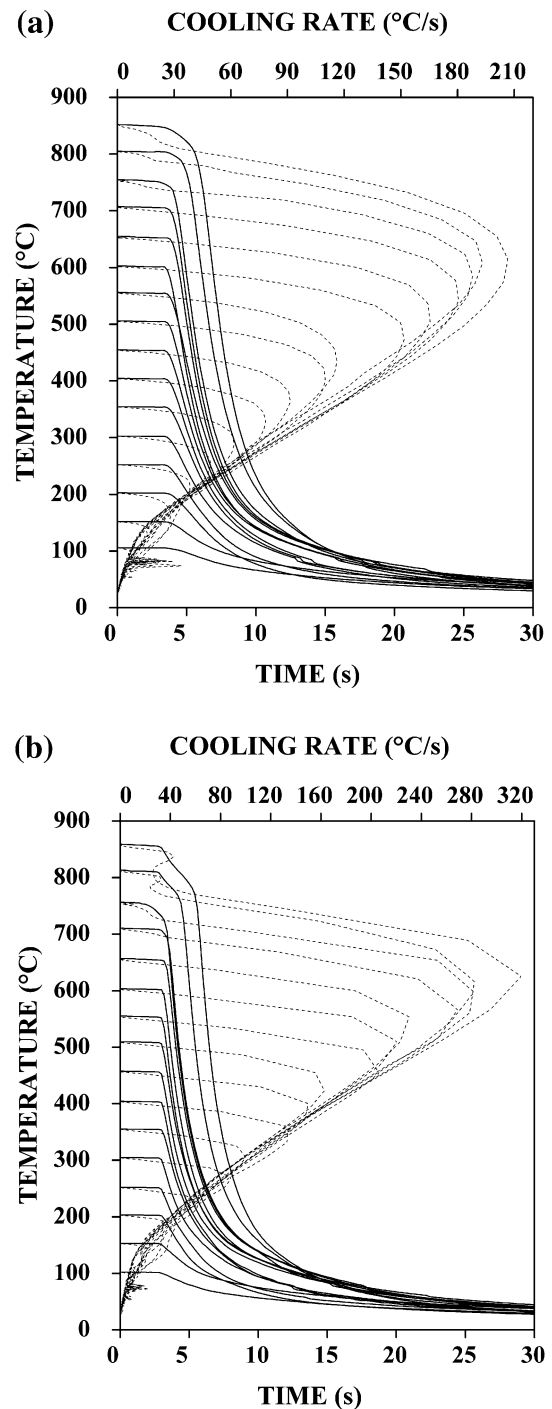


**Fig. 11** Thermal history (solid line) and cooling rate (dash line) curves of quench probe measured at **a** TC1 and **b** TC2 locations of probe during immersion cooling in water

were input to Eq. (6) to estimate mean cooling rates at the TC1 and TC2 locations of the probe. The mean cooling rates of experimentally measured time-temperature plots for different probe heating temperatures were also determined. Figure 15 shows the experimentally measured and numerically estimated mean cooling rates for the probe



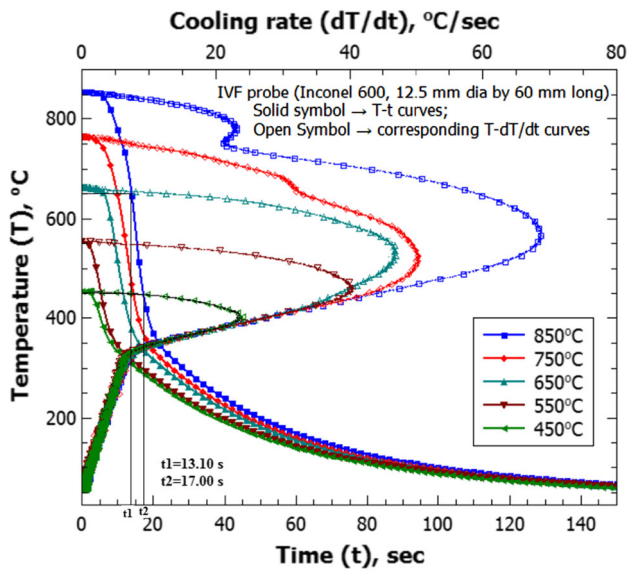


**Fig. 12** Thermal history and cooling rate curves obtained at the geometric centre of Inconel 600 probe quenched in mineral oil [13]

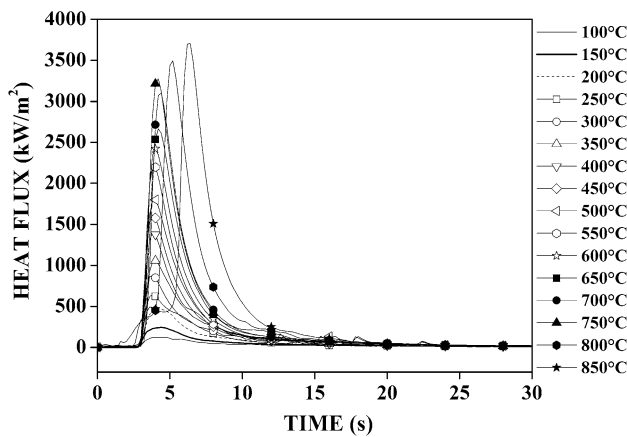


**Fig. 13** Estimated metal/quenchant interfacial heat flux transients for Inconel probe quenched in water

quenched from different temperatures. There was good agreement between the measured and estimated cooling rates.

The model was also validated with the available data reported in literature. The cooling curve plot (Fig. 12) presented by Maniruzzaman et al. [11] was used to calculate mean cooling rates for the Inconel 600 probe for the quench start temperatures of 750 and 850 °C. Typical calculation is shown as a solid black line for 850 °C in Fig. 12. The calculated mean cooling rates were about 40 and 51 °C/s for the quench start temperatures of 750 and 850 °C respectively. They reported the following relationship between maximum  $h$  ( $h_{max}$ ) and  $T_{start}$  for an

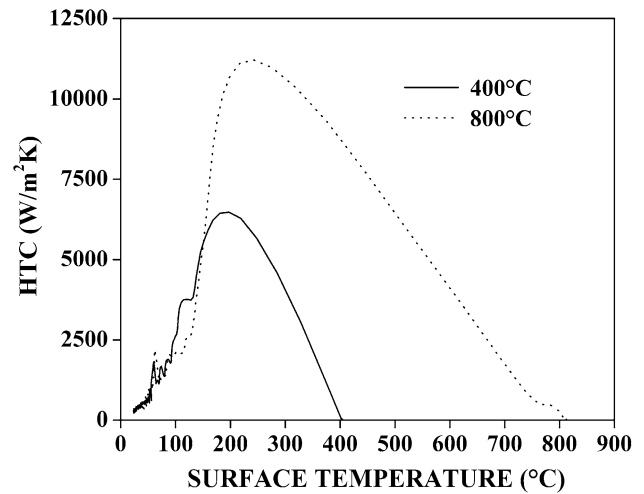


**Fig. 14** Calculated heat transfer coefficient for different probe quench start temperatures

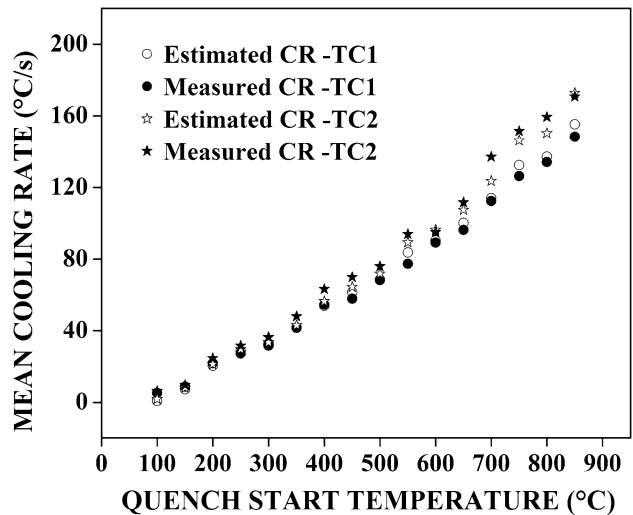


**Fig. 15** Estimated and measured mean cooling rates for different probe quench start temperatures

Inconel probe heated in the range of 450–850 °C quenching in mineral oil.

$$h_{max} = 2.1816T_{start} - 422.7206 \tag{9}$$

The above equation was used to determine  $h_{max}$  values for the probe quench start temperatures of 750 and 850 °C and they were found to be 1,213 and 1,432 W/m<sup>2</sup>K respectively. The corresponding mean heat transfer coefficients values were 854 and 1,008 W/m<sup>2</sup>K (In our study, the mean ratio of  $h$  to  $h_{max}$  was found to be 0.704). The mean heat transfer coefficients values for probe quench start temperatures of 750 and 850 °C were used as input to Eq. (6) to estimate the mean cooling rate at the centre of

the probe and were found to be 38.23 and 48.09 °C/s for the quench start temperatures of 750 and 850 °C respectively. The estimated cooling rates are in good agreement with the measured cooling rates, which confirm the validity of the proposed model.

The proposed methodology could be used effectively in metallurgical cooling processes such as quench hardening, continuous casting and metal forming to optimize the cooling conditions and thus obtain desired mechanical properties. For example, cooling conditions during quench hardening of steel has significant effect on the formation microstructure, mechanical properties and distortion of components. The cooling rate of the components should be more than the critical cooling rate (nose of TTT diagram) in-order to obtain a fully martensitic structure. Further, the cooling rate of the steel component initially should be fast enough to prevent austenite to ferrite/pearlite transformation whereas cooling in the martensitic range should be slow enough to prevent distortion and cracking of components. Hence proper cooling conditions during quench hardening of steel is necessary to obtain desired properties of the component without distortion and cracking. By using the proposed model, it is possible to predict the average cooling rate of the components obtained for a known quench medium. On the other-hand, for a material and required cooling rate, cooling severity required from the quench medium could be predicted and accordingly an appropriate quench medium can be selected. Further, the model also correlates the probe temperature and cooling rate and hence the cooling condition during quenching can be changed accordingly by the use of fresh cooling fluid and/or agitation of the fluid.

#### 4 Conclusions

Numerical simulation of heat transfer during cooling of Inconel 600 probe was carried out. The combined effects of the quench start temperature and boundary heat transfer coefficient on the cooling curve of the probe was assessed. The cooling rate increased with increase in heat transfer coefficient and the quench start temperature. Simulation results indicated the existence of a critical value of heat transfer coefficient below which the spatial variation of cooling rates was negligible. The value of the critical heat transfer coefficient increased with increase in quench start temperature.

Computer aided cooling curve analysis during quenching experiments indicated the formation of stable vapour blanket on quench probe surface above 750 °C. Below this temperature, film boiling phenomenon was not observed. The peak cooling rate of the probe increased with increase in quench start temperature. The magnitudes of cooling

rates up to the peak value were different and were influenced only by the quench start temperature. After the occurrence of peak, the probe temperature was the significant factor that determined the cooling rates clearly indicating the influence of quench start temperature only on film and transition boiling. The effect of quench start temperature of the material and the boundary heat transfer coefficient on mean cooling rate was modelled. The model was experimentally validated and would be useful in optimizing cooling conditions during quench heat treatment.

**Acknowledgments** One of the authors (KNP) thank the Science and Engineering Research Board (SERB), Department of Science and Technology (DST), New Delhi, India for funding this investigation under a research Grant.

#### References

1. Totten GE, Bates CE, Clinton NA (1993) Handbook of quenchants and quenching technology. ASM International, Materials Park, pp 239–289
2. Liscic B (1993) State of the art in quenching. In: Hodgson PD (ed) Quenching and carburizing. The Institute of Materials, London, pp 1–32
3. Liscic B, Tensi HM, Canale LCF, Totten GE (2010) Quenching theory and technology. CRC Press, Boca Raton, pp 159–178
4. Simsir C, Gur CH (2008) Simulation of quenching. In: Gur CH, Pan J (eds) Handbook of thermal process modeling steels. CRC Press, Boca Raton, pp 341–475
5. Mayer S, Scheu C, Leitner H, Clemens H, Siller I (2007) Influence of the cooling rate on the mechanical properties of a hot-work tool steel. BHM Berg- Huettenmaenn Mon 152:132–136
6. Tszeng TC, Wu WT, Tang JP (1996) Prediction of distortion during heat treating and machining processes. In: Dosselt JL & Luetje RE (Eds) Proceeding of the 16th ASM heat treating society conference and exposition, Ohio, pp 9–15
7. Sengupta J, Thomas BG, Wells MA (2005) The use of water cooling during the continuous casting of steel and aluminium alloys. Metall Mater Trans A 36:187–204
8. Bates CE, Totten GE, Brennan RL (1991) Quenching of steel. ASM handbook—heat treatment. ASM International, Materials Park, pp 160–291
9. Li D, Wells MA, Cockcroft SL, Caron E (2007) Effect of sample start temperature during transient boiling water heat transfer. Metall Mater Trans B 38:901–910
10. Babu K, Prasanna Kumar TS (2009) Mathematical modelling of surface heat flux during quenching. Metall Mater Trans B 41:214–224
11. Maniruzzaman M, Dai X, Sisson J (2012) Effect of quench start temperature on surface heat transfer coefficients. In: MacKenzie DS (Ed) Quenching control and distortion 2012: Proceedings of the 6th International Quenching and Control of Distortion Conference Including the 4th International Distortion Engineering Conference, Chicago, Illinois, USA. pp 57–68
12. Ramesh G, Prabhu KN (2012) Effect of boundary heat transfer coefficient and probe section size on cooling curves during quenching. Mater Perform Charact, 1: MPC104365
13. Ramesh G, Prabhu KN (2013) Dimensionless cooling performance parameter for characterization of quench media. Metall Mater Trans B 44:797–799

14. Kumar TS (2004) A serial solution for the 2-D inverse heat conduction problem for estimating multiple heat flux components. *Numer Heat Transf B: Fundam* 45:541–563
15. Penha RN, Canale LCF, Totten GE, Sarmiento GS, Ventura JM (2006) Simulation of heat transfer and residual stresses from cooling curves obtained in quenching studies. *J ASTM Int* 3: JA113614
16. Grum J, Bozic S, Zupanc M (2001) Influence of quenching process parameters on residual stresses in steel. *J Mater Process Technol* 114:57–70
17. Funatani K, Narazaki M, Tanaka M (1999) Comparisons of probe design and cooling curve analysis methods. In: Midea SJ, Pfaffmann GD (Eds) 19th ASM heat treating society conference proceedings including steel heat treatment in the new millennium November 1–4, Cincinnati, Ohio, pp 255–263